PAPER

Check for updates

Critical conditions for the formation of p-type ZnO with Li doping

Mingge Jin, [ab] Zhibing Li,[a] Feng Huang, [b] Yu Xia,[a] Xu Ji[b] and Weiliang Wang [*a]

The stability of Li dopants in ZnO is studied *via* first-principles calculations with electric dipole correction. The formation energies of substitutional Li (Li_{Zn}), interstitial Li (Li_i) and the $Li_{Zn} + Li_i$ complex are calculated in large supercells and the results are extrapolated to the limit of an infinite-sized supercell. The stabilities of $2Li_{Zn}$ and the $Li_{Zn} + Li_i$ complex are found to depend on the temperature and absolute oxygen partial pressure. At normal experimental temperature (900 K), an extremely high absolute oxygen partial pressure (194 bar) is needed to break the coupling between Li_{Zn} and Li_i and thus form p-type ZnO. The reaction barrier and the absorbance spectra are also discussed.

1 Introduction

ZnO is considered as a promising candidate for high-efficiency UV electroluminescence at room temperature due to its large exciton binding energy (60 meV) and wide band gap (3.37 eV).[1,2] The well-known bottleneck for the electroluminescence of ZnO is obtaining stable p-type ZnO with a high carrier concentration (HCC).[3]

Since 2000, in order to obtain the desired p-type ZnO, *via* creating shallow acceptors, with a concentration higher than that of the total donors, doping Li has become one of the major efforts. It was demonstrated that Li substituting Zn (Li_{Zn}) could work as a shallow acceptor with an activation energy of 0.09 eV.[4,5] Theoretically, if Li_{Zn} possessed sufficiently large-concentration shallow acceptors (larger than the total donors created by other uncontrollable factors), the desired p-type ZnO stable at room temperature would be achieved. However, in experiment, Li doped p-type HCC-ZnO is still far from success.[6–9] It was found that interstitial Li (Li_i) is always formed with a concentration commensurate to that of Li_{Zn} during the doping process. As we know, Li_i, acting as a shallow donor, will compensate acceptor Li_{Zn} and finally form I-type ZnO.[10,11] Actually, the simultaneous concentration increase of two defects (Li_{Zn} and Li_i) with different formation energies is an abnormal thermodynamic phenomenon, which implies that Li_{Zn} and Li_i may be correlated and act as an integrated defect in ZnO. In awareness of the above fact, researchers[11–13] had begun to study the stability of Li_{Zn}, Li_i and the $Li_{Zn} + Li_i$ defect complex under different thermodynamic conditions using first-principles calculations. The common agreement was, in most

normal thermodynamic conditions, that the $Li_i + Li_{Zn}$ defect complex was more stable than the single defects Li_{Zn} and Li_i. The argument was whether the relative stability of the $Li_{Zn} + Li_i$ defect complex and Li_{Zn} would change with the variation of oxygen chemical potential. According to R. Vidya *et al.*,[12] the oxygen chemical potential is dependent on the percentage of the oxygen partial pressure. They showed that $Li_{Zn} + Li_i$ transformed into $2Li_{Zn}$ when the oxygen partial pressure is 80% of the total pressure, leading to p-type ZnO. However, their result is inconsistent with the experiments. In fact, the chemical potential of oxygen in thermodynamic equilibrium is not dependent on the percentage of the partial pressure, but on the absolute partial pressure as well as temperature. The dependence on pressure and temperature has never been studied in previous researches. To study this, we focus on the absolute partial pressure, instead of the percentage.

In this work, based on the density functional theory (DFT) calculations, the formation energies of Li_{Zn}, Li_i and $Li_{Zn} + Li_i$ defect complex at different temperature and absolute oxygen partial pressure are calculated in large supercells. The electric dipole correction and the limit of infinite-sized supercell are considered. The results show that the stability of $2Li_{Zn}$ and $Li_{Zn} + Li_i$ defect complex depends on the temperature and absolute oxygen partial pressure. Furthermore, it is indicated that at normal experimental temperature (900 K), an extremely high absolute oxygen partial pressure (194 bar) is needed to break the coupling between Li_{Zn} and Li_i, for the formation of p-type ZnO. Our conclusion is much consistent with experiments,[14] suggesting that Li-doped p-type ZnO might be realized by annealing samples under positive oxygen partial pressure. Our study also reveals that long-range electrostatic interactions between different dopants will decisively influence the thermodynamically stable conditions of Li defects in ZnO, which implies that the supercell size effect should be fully considered in the future theoretical work.

[a]State Key Laboratory of Optoelectronic Materials and Technologies, School of Physics, Guangdong Province Key Laboratory of Display Material and Technology, Sun Yat-sen University, Guangzhou 510275, People's Republic of China. E-mail: wangwl2@mail.sysu.edu.cn

[b]State Key Laboratory of Optoelectronic Materials and Technologies, School of Materials, Sun Yat-sen University, Guangzhou, 510275, People's Republic of China

2 Theory and computational details

The DFT calculations are performed by Vienna Ab initio Simulation Package (VASP)[15–17] using the projector augmented-wave (PAW) method.[18] Periodic boundary condition is applied. Different Li dopants in wurtzite ZnO (w-ZnO) are considered: Li atoms substitute Zn atoms (Li_{Zn}), Li atoms occupy octahedral interstitial sites (Li_i^{oct}) or tetrahedral site (Li_i^{tet}), $Li_{Zn} + Li_i^{oct}$ and $Li_{Zn} + Li_i^{tet}$ (Fig. 1). All atoms are fully relaxed until all forces acting on atoms are smaller than 0.01 eV Å^{-1}. The Perdew–Burke–Ernzerhof (PBE)[19] generalized gradient approximation (GGA) functional is used for the exchange correlation potential. The cut-off energy for the plane-wave expansion is 400 eV. For the Brillouin zone integration, we use a $3 \times 3 \times 3$ k-point Monkhorst–Pack mesh for $3 \times 3 \times 2$, $4 \times 4 \times 2$ and $4 \times 4 \times 3$ supercells, and a Γ-point calculation for $4 \times 4 \times 4$ and $6 \times 6 \times 4$ supercells. We have calculated the energies for denser k-points mesh and find that the energy differences are less than 0.001 eV, which indicates the meshes are dense enough.

The transition state calculation is done by Nudged Elastic Band (NEB) method[20] in $3 \times 3 \times 2$ supercell. The climbing method is applied.[21] The absorbance spectra are also calculated with $3 \times 3 \times 2$ supercell.

2.1 Dopant formation energy

The formation energy of Li_{Zn} or Li_i is:[22]

$$E_f = E_t^d - E_t^p + n_{Zn}[E_{Zn} + \mu_{Zn}(T,p)] - n_{Li}[E_{Li} + \mu_{Li}(T,p)], \quad (1)$$

where E_t^d and E_t^p denote the total energies of Li-doped and undoped ZnO, respectively. n_{Zn} (n_{Li}) is the number of Zn (Li) atoms added to or removed from the supercell. E_{Zn} (E_{Li}) is the single atom energy in solid Zn (Li). μ_{Zn} (μ_{Li}) is the chemical potential of Zn (Li) atom which depends on the experimental conditions (temperature and partial pressure). The formation energy is actually defined as the Gibbs free energy difference between the product and the reactant. Therefore, the chemicals with lower formation energy will be produced after chemical reactions under given pressure and temperature.

Chemical potential of Zn is determined by that of O_2 and ZnO

$$\mu_{Zn} = \mu_{ZnO}(T,p^0) - \frac{1}{2}\mu_{O_2}(T,p_{O_2}). \quad (2)$$

The chemical potentials of gaseous O_2 is given by

$$\mu_{O_2}(T,p_{O_2}) = \mu_{O_2}(T,p^0) + k_B T \ln\left(\frac{p_{O_2}}{p^0}\right), \quad (3)$$

where $p^0 = 1$ bar, and p_{O_2} is the absolute oxygen partial pressure. $\mu_{ZnO}(T,p^0)$ and $\mu_{O_2}(T,p^0)$ had been measured by experimentalists and can be looked up in ref. 23–25.

There is a charge-state term qE_f in eqn (1) according to some literatures (e.g. ref. 12 and 26). It is wrong to include the charge-state term in calculation of bulk ZnO. The reasons are shown below.

(1) The Fermi level is not a tunable parameter in ZnO growth experiments, as determined by the density of states and total number of electrons, unless when studying chemical reactions on electrode (e.g. ref. 27). It is not a common practice to put an electrode into the reaction chamber when doping ZnO at high oxygen pressure and high temperature. Therefore, experimentalists are actually not able to tune the Fermi level during the growth of ZnO.

(2) It is not wise to simulate charge-state in crystal in periodic boundary condition, as the total charge in the supercell should be zero in such situation. VASP (the software ref. 12 and 26 and our work used) assumes a homogeneous positive background-charge when an extra electron is put into the supercell. This would introduce artificial error.

(3) The extra electron in the supercell may not be bound near the impurity to form "charge-state", when an extra electron is put into the supercell and vice versa.
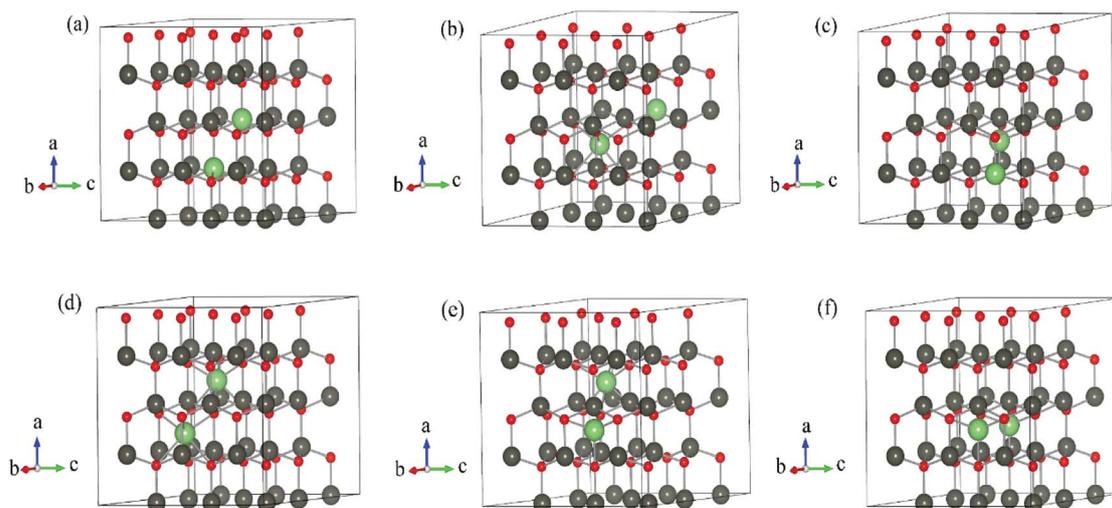

Fig. 1 Schematic illustration of $3 \times 3 \times 2$ supercells of w-ZnO: (a) $2Li_{Zn}$, (b) $Li_{Zn} + Li_i^{oct}$, (c) $Li_{Zn} + Li_i^{tet}$, (d) $2Li_i^{oct}$, (e) $Li_i^{oct} + Li_i^{tet}$ and (f) $2Li_i^{tet}$. The grey, red and green balls represent Zn, O and Li atoms, respectively.

2.2 Electric dipole correction

Since the total energies are calculated with periodic boundary condition, artificial long-range electrostatic interactions between the periodic defect images should be subtracted. By introducing the electric dipole correction,[28,29] the artificial effect can be mostly eliminated. The interaction energy between two electric dipole moments is given by

$$U = \frac{1}{2}\sum_{i \neq j}\frac{\vec{p}_i \cdot \vec{p}_j - 3(\vec{p}_i \cdot \hat{r}_{ij})(\vec{p}_j \cdot \hat{r}_{ij})}{4\pi\varepsilon_0 r_{ij}^3} = \frac{1}{2}\sum_{i \neq j}\frac{\vec{p}^2 - 3(\vec{p} \cdot \hat{r}_{ij})^2}{4\pi\varepsilon_0 r_{ij}^3},$$

(4)

where $\hat{r}_{ij} = \vec{r}/r$ is the unit vector pointing from dipole i to dipole j, ε_0 is the dielectric constant of vacuum, and $\vec{p}_i$ is the electric dipole moment in the i-th supercell. The electric dipoles in each supercell are the same (periodic boundary condition), denoted by $\vec{p}$.

3 Results and discussion

3.1 Formation energy vs. supercell size

We have calculated the energy of each dopant with $3 \times 3 \times 2$, $4 \times 4 \times 2$, $4 \times 4 \times 3$, $4 \times 4 \times 4$ and $6 \times 6 \times 4$ supercells. The corresponding atom numbers for undoped ZnO in these supercells are 72, 128, 192, 256 and 576 respectively. The dopant concentrations for two Li atoms doping in these supercells are 2.78 at%, 1.55 at%, 1.04 at%, 0.78 at% and 0.35 at% respectively.

Among those interstitial sites shown in Fig. 1d–f, Li prefers to occupy the octahedral interstitial site (Li_i^{oct}) at which it forms six bonds with neighboring atoms. Four different cases of Li doping configurations: (i) $2Li_{Zn}$, (ii) $Li_{Zn} + Li_i^{oct}$, (iii) $Li_{Zn} + Li_i^{tet}$ and (iv) $2Li_i^{oct}$ are considered. Two dopants locating at the nearest (N) sites and separating from each other (S) are considered for each of these configurations. The formation energies of these configurations are shown in Fig. 2 as functions of Li doping concentration at 0 K (*i.e.* $\mu_{Zn} = \mu_{Li} = 0$).

The formation energies converge very slowly in regard to decreasing Li doping concentration (increasing supercell size) due to the large electric dipole moments induced by the dopants. Therefore, we apply the dipole correction to remove the artificial long-range electrostatic interactions between different dopants. The formation energies with dipole correction converge to constant in low Li concentration (open symbols in Fig. 2). As shown in Fig. 2, Li atoms in $2Li_{Zn}$ and $2Li_i^{oct}$ prefer S configuration, while the Li atoms in $Li_{Zn} + Li_i$ pair prefer N configuration.

3.2 Formation energy vs. absolute oxygen partial pressure (with dipole correction)

As $2Li_{Zn}$ is the only case of p-type doping among our investigated various dopants, it is essential to find out the chemical environment for $2Li_{Zn}$ to be the most stable one. The relative stability of different Li doping configurations is determined by the growth temperature and absolute oxygen partial pressure.
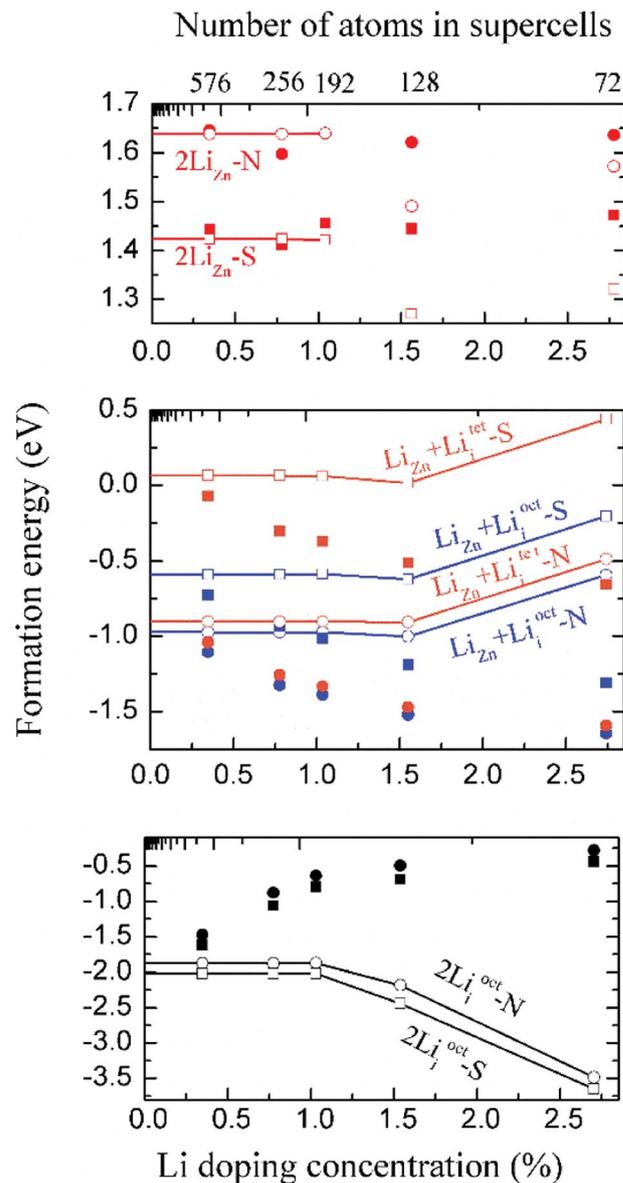

Fig. 2 Formation energies without (filled) and with (open) dipole correction of (i) $2Li_{Zn}$ (red), (ii) $Li_{Zn} + Li_i^{oct}$ (blue), (iii) $Li_{Zn} + Li_i^{tet}$ (orange) and (iv) $2Li_i^{oct}$ (black) in ZnO when the temperature is 0 K (*i.e.* $\mu_{Zn} = \mu_{Li} = 0$). N and S indicate two dopants locating at the nearest sites and separating from each other, respectively.

This is illustrated in Fig. 3, where we show the formation energies of the three most stable configurations.

As shown in Fig. 3, Li dopant will be mainly in interstitial form at low absolute oxygen partial pressure. The compensating $Li_{Zn} + Li_i$ pair is always the most stable configuration near the standard pressure ($p_{O_2} = 1$ bar), which implies that $Li_{Zn} + Li_i$ is stable for most of the growth condition (at a moderate p_{O_2}). The configuration $2Li_{Zn}$ forms at high p_{O_2}.

Critical absolute oxygen partial pressure $p_{O_2}^{(1)}$ and $p_{O_2}^{(2)}$ for alternating the stability of the three configurations are listed in Table 1. $p_{O_2}^{(1)}$ ($p_{O_2}^{(2)}$) corresponds to the crossover points of the black lines and blue lines (blue lines and red lines) in Fig. 3. It
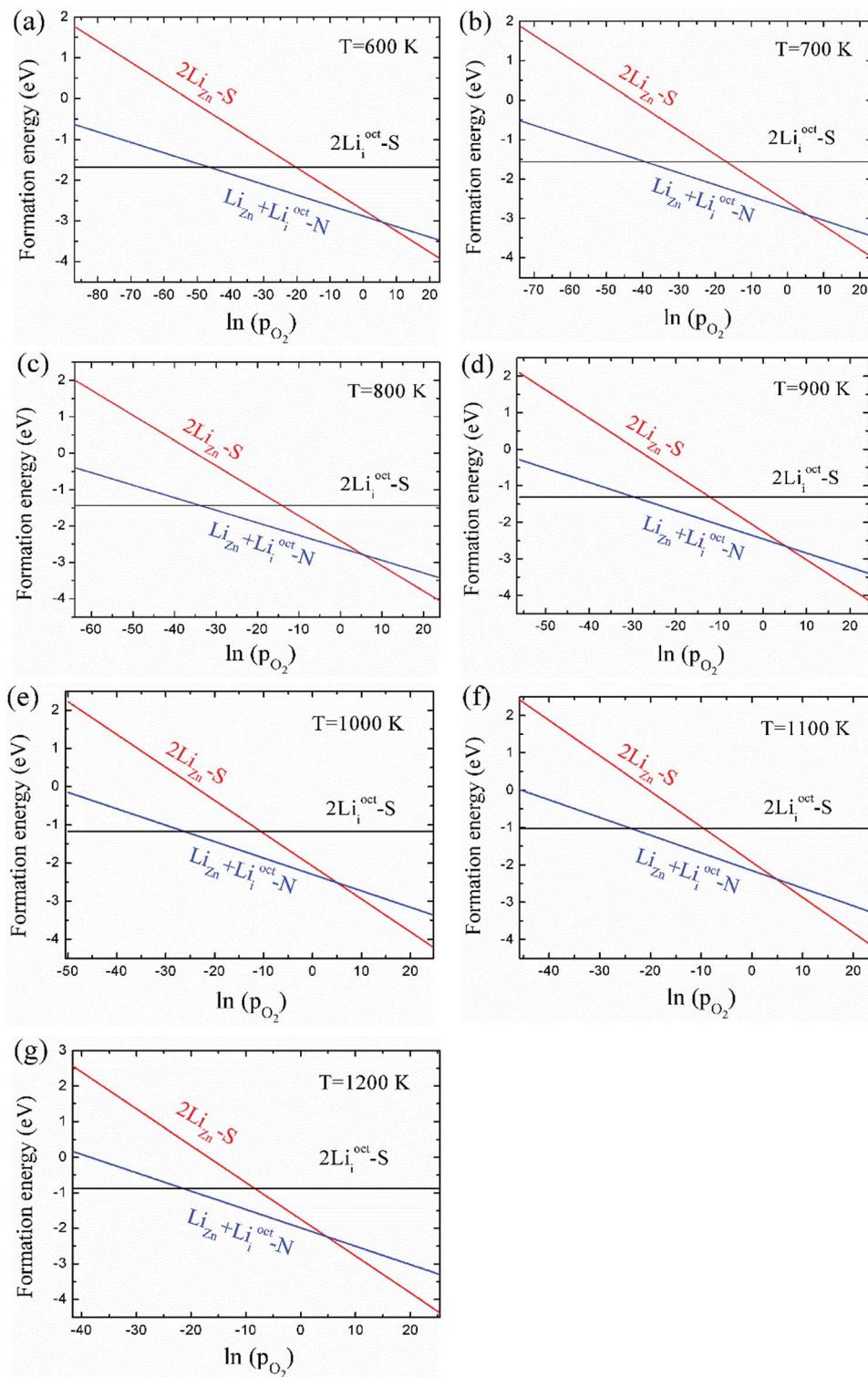
Fig. 3 Formation energies of the three most stable configurations as the function of absolute oxygen partial pressure p_{O_2} (unit: bar) at different temperatures. The dependence on oxygen chemical potential has been converted into the absolute oxygen partial pressure dependence at given temperature.

can be seen that the minimum of oxygen partial pressure $(p_{O_2}^{(2)})$ required for $2Li_{Zn}$ being the most stable defect decreases with increasing temperature. On the other hand, the maximum of oxygen partial pressure $(p_{O_2}^{(1)})$ allowed for $2Li_i$ being the most stable defect increases with increasing temperature. Phase diagram of the three configurations is shown in Fig. 4.

Table 1 Critical absolute oxygen partial pressure $p_{O_2}^{(1)}$ and $p_{O_2}^{(2)}$ for alternating the stability of the three configurations. $p_{O_2}^{(1)}$ ($p_{O_2}^{(2)}$) corresponds to the crossover points of the black lines and blue lines (blue lines and red lines) in Fig. 3

T (K)	μ_{ZnO} (eV)	$\mu_{O_2}(T,p^0)$ (eV)	$p_{O_2}^{(1)}$ (bar)	$p_{O_2}^{(2)}$ (bar)
600	−0.245	−1.296	6.25×10^{-21}	319.402
700	−0.324	−1.492	8.95×10^{-18}	260.962
800	−0.411	−1.711	2.37×10^{-15}	254.947
900	−0.503	−1.923	1.41×10^{-13}	194.368
1000	−0.602	−2.152	3.95×10^{-12}	166.831
1100	−0.705	−2.376	5.12×10^{-11}	124.633
1200	−0.814	−2.625	5.05×10^{-10}	114.18

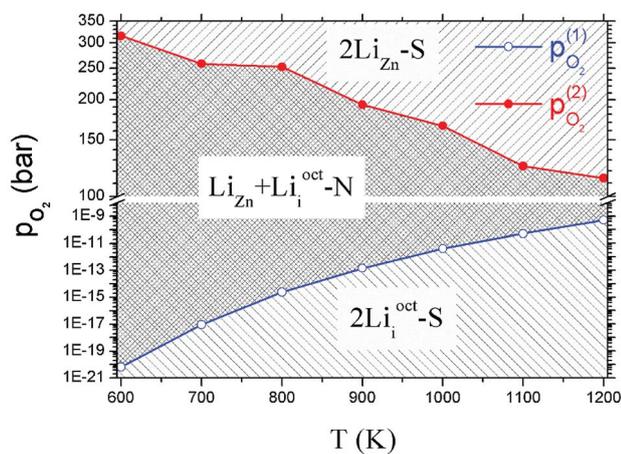**Fig. 4** Phase diagram of Li doped ZnO. The blue dots and red dots indicate the values of $p_{O_2}^{(1)}$ and $p_{O_2}^{(2)}$ at different temperatures. The most stable defect in the region above the red line is $2Li_{Zn}$-S, between the red line and blue line is $Li_{Zn} + Li_i^{oct}$-N, and below the blue line is $2Li_i^{oct}$-S.

Table 2 The same as Table 1 but without dipole correction

T (K)	$p_{O_2}^{(1)}$ (bar)	$p_{O_2}^{(2)}$ (bar)
600	7.20×10^{-30}	1.05×10^5
700	1.95×10^{-25}	3.74×10^4
800	4.69×10^{-22}	1.97×10^4
900	1.55×10^{-19}	9.25×10^3
1000	1.71×10^{-17}	5.40×10^3
1100	6.82×10^{-16}	2.94×10^3
1200	1.71×10^{-14}	2.07×10^3

3.3 Formation energy *vs.* absolute oxygen partial pressure (without dipole correction)

In this section, we show the results without dipole correction for comparison with Table 2 and Fig. 5. It can be seen that the critical absolute oxygen partial pressure $p_{O_2}^{(1)}$ and $p_{O_2}^{(2)}$ for alternating the stability of the three configurations are changed one to three orders of magnitude by the dipole correction. Therefore, it is essential to apply the dipole correction.
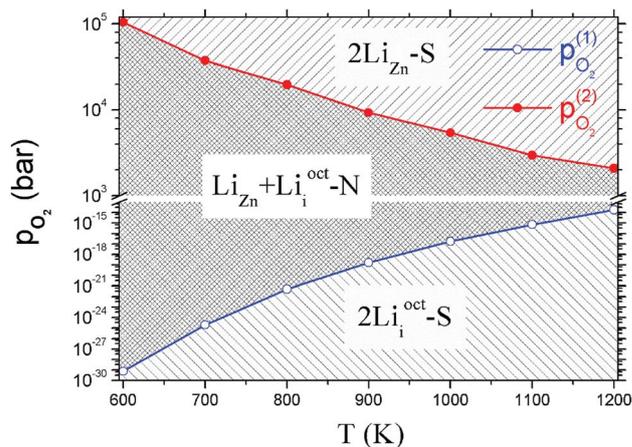

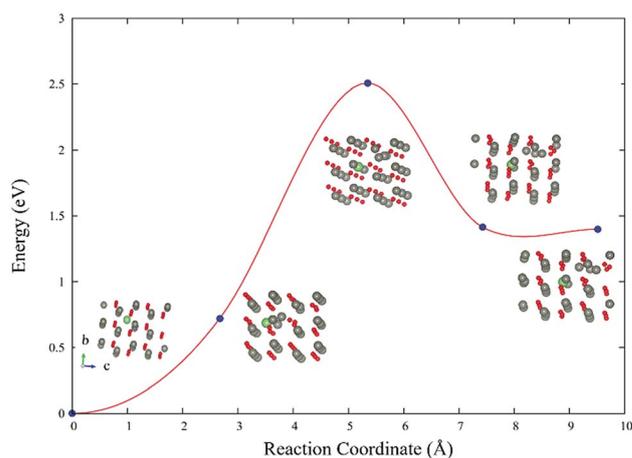**Fig. 5** The same as Fig. 4 but without dipole correction.

Fig. 6 Reaction barrier of $Li_{Zn} + Li_i \rightarrow 2Li_{Zn} + Zn$.

3.4 Reaction barrier

The reaction barrier of $Li_{Zn} + Li_i \rightarrow 2Li_{Zn} + Zn$ is 2.5 eV (Fig. 6). Therefore $Li_{Zn} + Li_i$ is easy to transform into $2Li_{Zn} + Zn$ when the temperature is 900 K. Although the reaction barrier of the reverse reaction $2Li_{Zn} + Zn \rightarrow Li_{Zn} + Li_i$ is even lower (1.1 eV), this reverse reaction will be blocked after the sample is annealed in high oxygen which eliminates the extra Zn.

3.5 Spectroscopic properties

We calculated the absorbance spectra of Li-doped ZnO. The bottom of conduction band is filled with electrons in Li-doped ZnO with Li_i configuration (n-type) (Fig. 7e). The electrons can not hop to the bottom of conduction band and have to hop to higher energy levels instead. Therefore, there is blue shift in absorbance spectrum (Fig. 7b) of n-type ZnO due to the band-filling effect. The top of valence band is empty in Li-doped ZnO with Li_{Zn} configuration (p-type) (Fig. 7f). There is red shift in absorbance spectrum (Fig. 7c) of p-type ZnO due to the internal hopping in the valence band. Our calculation results can not explain the blue shift in the absorbance spectra of N-
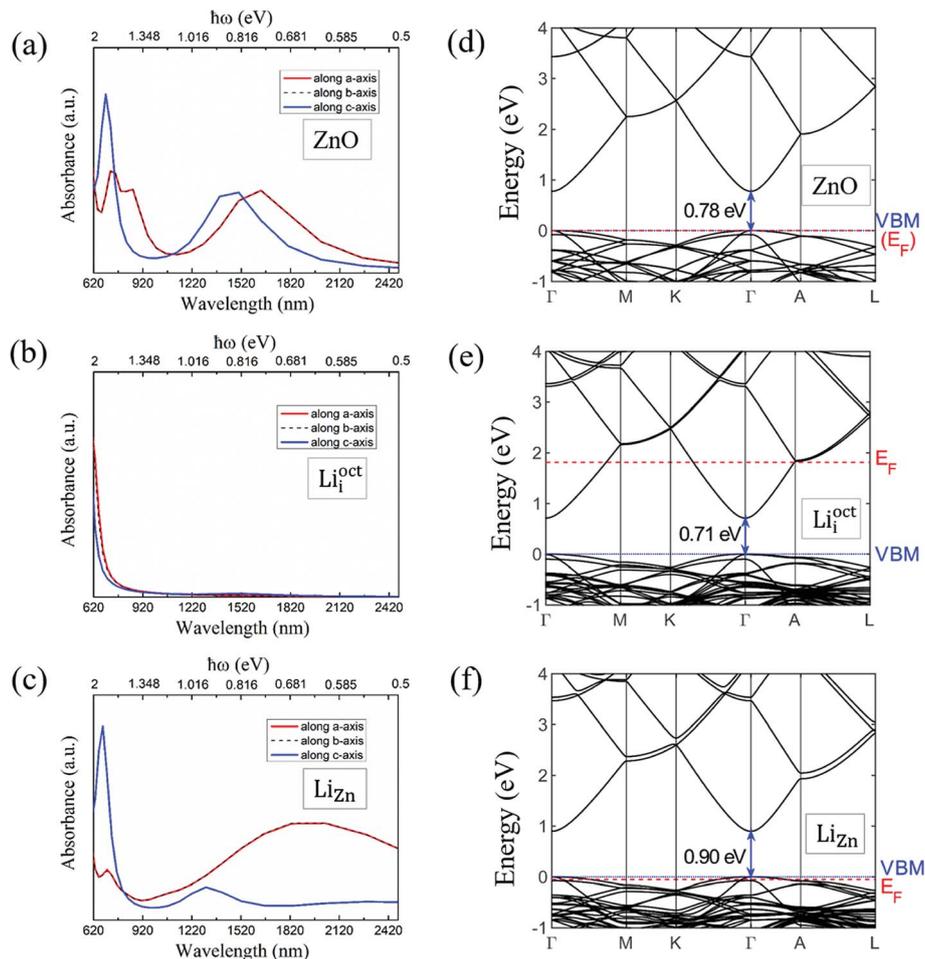
Fig. 7 Absorbance spectrum of (a) pure ZnO and Li-doped ZnO with (b) Li_i configuration and (c) Li_{Zn} configuration. The polarizations of light in a, b and c directions are considered. Band structure of (d) pure ZnO and Li-doped ZnO with (e) Li_i configuration and (f) Li_{Zn} configuration.

doped ZnO if it is p-type.[30] The experimental results in ref. 30 demands more detailed theoretical investigation.

4 Conclusions

First-principles calculations have been performed to study the formation energies of Li dopants in ZnO at different temperature and absolute oxygen partial pressure. Four different Li dopant configurations have been investigated in large supercell containing up to 576 atoms with electric dipole correction. It is found that the formation energy for defect complexes (Li_{Zn} + Li_i^{oct} N-pair and Li_{Zn} + Li_i^{oct} S-pair) is not converged until the supercell is larger than $4 \times 4 \times 3$.

The stability of $2Li_{Zn}$ and Li_{Zn} + Li_i complex depends on the temperature and absolute oxygen partial pressure. At low temperature, we find that Li dopant will be mainly in the compensating Li_{Zn} + Li_i form. At the normal experimental temperature (900 K), an extremely high absolute oxygen partial pressure (194 bar) is needed to break the coupling between Li_{Zn} and Li_i and form the p-type $2Li_{Zn}$. This result is in very good agreement with recent experiments,[14] suggesting that Li-doped p-type ZnO might be realized by annealing samples under

positive oxygen partial pressure, which can not be achieved in MOCVD and MBE with negative pressure. This explains why good p-type ZnO can not be synthesized before.

Our study also reveal that long-range electrostatic interactions between different dopants will decisively influence the thermodynamical stability of Li dopants in ZnO, which implies that the supercell size effect should be fully considered in the future theoretical work.

The reaction barrier of Li_{Zn} + Li_i → $2Li_{Zn}$ + Zn is 2.5 eV, which is easy for Li_{Zn} + Li_i to transform into $2Li_{Zn}$ + Zn when the temperature is 900 K. There is blue shift in absorbance spectrum of n-type ZnO due to the band-filling effect; there is red shift in absorbance spectrum of p-type ZnO due to the internal hopping in the valence band.

Author contributions

M. J. performed all the first-principles calculations with the help from Y. X. and W. W., while Z. L. provided the idea of dipole correction. F. H. and X. J. proposed the topic of Li doped ZnO. M. J., F. H. and W. W. wrote the introduction. M. J. and W. W. analyzed the results and wrote the other part of the

paper. Y. X. and X. J. participated in final correction of the manuscript. All authors read and approved the final manuscript.

Conflicts of interest

There are no conflicts to declare.

Acknowledgements

References

1 Ü. Özgür, Y. I. Alivov, C. Liu, A. Teke, M. Reshchikov, S. Doğan, V. Avrutin, S.-J. Cho and H. Morkoc, *J. Appl. Phys.*, 2005, **98**, 11.

2 J. C. Fan, K. Sreekanth, Z. Xie, S. Chang and K. V. Rao, *Prog. Mater. Sci.*, 2013, **58**, 874–985.

3 V. Avrutin, D. J. Silversmith and H. Morkoç, *Proc. IEEE*, 2010, **98**, 1269–1280.

4 C. Park, S. Zhang and S.-H. Wei, *Phys. Rev. B: Condens. Matter Mater. Phys.*, 2002, **66**, 073202.

5 E.-C. Lee and K. Chang, *Phys. Rev. B: Condens. Matter Mater. Phys.*, 2004, **70**, 115210.

6 J. Lu, Y. Zhang, Z. Ye, Y. Zeng, H. He, L. Zhu, J. Huang, L. Wang, J. Yuan and B. Zhao, *Appl. Phys. Lett.*, 2006, **89**, 112113.

7 Y. Zeng, Z. Ye, W. Xu, D. Li, J. Lu, L. Zhu and B. Zhao, *Appl. Phys. Lett.*, 2006, **88**, 062107.

8 J. Lee, S. Cha, J. Kim, H. Nam, S. Lee, W. Ko, K. L. Wang, J. Park and J. Hong, *Adv. Mater.*, 2011, **23**, 4183–4187.

9 S. Chawla, K. Jayanthi and R. Kotnala, *Phys. Rev. B: Condens. Matter Mater. Phys.*, 2009, **79**, 125204.

10 A. Carvalho, A. Alkauskas, A. Pasquarello, A. Tagantsev and N. Setter, *Phys. Rev. B: Condens. Matter Mater. Phys.*, 2009, **80**, 195205.

11 M. Wardle, J. Goss and P. Briddon, *Phys. Rev. B: Condens. Matter Mater. Phys.*, 2005, **71**, 155205.

12 R. Vidya, P. Ravindran and H. Fjellvåg, *J. Appl. Phys.*, 2012, **111**, 123713.

13 J. Yi, C. Lim, G. Xing, H. Fan, L. Van, S. Huang, K. Yang, X. Huang, X. Qin and B. Wang, *Phys. Rev. Lett.*, 2010, **104**, 137201.

14 X. Ji, L. Chen, M. Xu, M. Dong, K. Yan, S. Cheng, X. Kong, T. Wang, J. Liu and B. Gu, *Adv. Electron. Mater.*, 2018, **4**, 1700307.

15 G. Kresse and J. Hafner, *Phys. Rev. B: Condens. Matter Mater. Phys.*, 1993, **48**, 13115.

16 G. Kresse and J. Furthmüller, *Phys. Rev. B: Condens. Matter Mater. Phys.*, 1996, **54**, 11169.

17 G. Kresse and D. Joubert, *Phys. Rev. B: Condens. Matter Mater. Phys.*, 1999, **59**, 1758.

18 P. E. Blöchl, *Phys. Rev. B: Condens. Matter Mater. Phys.*, 1994, **50**, 17953.

19 J. P. Perdew, K. Burke and M. Ernzerhof, *Phys. Rev. Lett.*, 1996, 77, 3865.

20 H. Jónsson, G. Mills and K. W. Jacobsen, *Nudged elastic band method for finding minimum energy paths of transitions*, 1998.

21 G. Henkelman, B. P. Uberuaga and H. Jónsson, *J. Chem. Phys.*, 2000, **113**, 9901–9904.

22 S. Horzum, D. Çakır, J. Suh, S. Tongay, Y.-S. Huang, C.-H. Ho, J. Wu, H. Sahin and F. Peeters, *Phys. Rev. B: Condens. Matter Mater. Phys.*, 2014, **89**, 155433.

23 I. Barin and G. Platzki, *Thermochemical data of pure substances*, Wiley Online Library, 1989.

24 W. M. Haynes, *CRC handbook of chemistry and physics*, CRC press, 2014.

25 *J. Phys. Chem. Ref. Data 14*, ed. M. Chase Jr, 1985.

26 S. Chen, J.-H. Yang, X.-G. Gong, A. Walsh and S.-H. Wei, *Phys. Rev. B: Condens. Matter Mater. Phys.*, 2010, **81**, 245204.

27 S. Zhou, N. Liu, Z. Wang and J. Zhao, *ACS Appl. Mater. Interfaces*, 2017, **9**, 22578–22587.

28 S. Giovanazzi, A. Görlitz and T. Pfau, *Phys. Rev. Lett.*, 2002, **89**, 130401.

29 J. H. Wesenberg and K. Mølmer, *Phys. Rev. Lett.*, 2004, **93**, 143903.

30 N. P. Herring, L. S. Panchakarla and M. S. Elshall, *Langmuir*, 2014, **30**, 2230.